Acta Neurochirurgica (2019) 161:2181–2193
https://doi.org/10.1007/s00701-019-04005-0

ORIGINAL ARTICLE - SPINE - OTHER

Augmented reality in intradural spinal tumor surgery

Barbara Carl[1] · Miriam Bopp[1,2] · Benjamin Saß[1] · Mirza Pojskic[1] · Christopher Nimsky[1,2]

Received: 6 June 2019 / Accepted: 5 July 2019 / Published online: 12 July 2019

Abstract

Background Microscope-based augmented reality (AR) is commonly used in cranial surgery; however, until recently, this technique was not implemented for spinal surgery. We prospectively investigated, how AR can be applied for intradural spinal tumor surgery.

Methods For ten patients with intradural spinal tumors (ependymoma, glioma, hemangioblastoma, meningioma, and metastasis), AR was provided by head-up displays (HUDs) of operating microscopes. User-independent automatic AR registration was established by low-dose intraoperative computed tomography. The objects visualized by AR were segmented in preoperative imaging data; non-linear image registration was applied to consider spine flexibility.

Results In all cases, AR supported surgery by visualizing the tumor outline and other relevant surrounding structures. The overall AR registration error was 0.72 ± 0.24 mm (mean ± standard deviation), a close matching of visible tumor outline and AR visualization was observed for all cases. Registration scanning resulted in a low effective dose of 0.22 ± 0.16 mSv for cervical and 1.68 ± 0.61 mSv for thoracic lesions. The mean HUD AR usage in relation to microscope time was 51.6 ± 36.7%. The HUD was switched off and turned on again in a range of 2 to 17 times (5.7 ± 4.4 times). Independent of the status of the HUD, the AR visualization was displayed on monitors throughout surgery.

Conclusions Microscope-based AR can be reliably applied to intradural spinal tumor surgery. Automatic AR registration ensures high precision and provides an intuitive visualization of the extent of the tumor and surrounding structures. Given this setting, all advanced multi-modality options of cranial AR can also be applied to spinal surgery.

Keywords Augmented reality · Head-up displays · Intradural spinal tumor surgery · Intraoperative computed tomography · Low-dose computed tomography · Spine registration

This article is part of the Topical Collection on *Spine - Other*

✉ Barbara Carl
carlb@med.uni-marburg.de

Miriam Bopp
bauermi@med.uni-marburg.de

Benjamin Saß
sassb@med.uni-marburg.de

Mirza Pojskic
mirza.pojskic@uk-gm.de

Christopher Nimsky
nimsky@med.uni-marburg.de

[1] Department of Neurosurgery, University Marburg, Baldingerstrasse, 35033 Marburg, Germany

[2] Marburg Center for Mind, Brain and Behavior (MCMBB), Marburg, Germany

Introduction

For more than 20 years, augmented reality (AR) based on head-up displays (HUD) of operating microscopes is clinically available. These systems, invented in the mid-1980s [17, 32], integrating operating microscopes HUDs into navigational setups to display and superimpose objects in the optical viewing field were initially known as microscope-based navigation [12, 18, 19, 27]. Nowadays, sophisticated microscope-based AR is routinely used in many centers for cranial neurosurgery [4–6, 8, 24]. Multimodal image data are integrated in these setups allowing to visualize not only anatomical and structural information, but also information related to function and metabolism [14, 29, 30].

Until recently, however, microscope-based AR was not available for spinal applications. After the feasibility of operating microscope HUD-based AR for spine surgery was shown in experimental settings in a case report on cervical foraminotomy [35] and in a cadaver study visualizing

osteotomy planes [20], we have implemented AR support for spine surgery using commercially system components [7]. The aim of this study is to investigate how microscope-based AR can be applied for surgery of intradural spinal tumors in an initial series of procedures.

Materials and methods

Between July 2018 and April 2019, 10 patients (7 females, 3 males; age range 36–84 years) underwent AR supported surgery for intradural tumors of the spine. Patient data and procedure details are summarized in Table 1. Informed consent was obtained from all individual participants included in this prospective observational study. We obtained ethics approval for prospective archiving clinical and technical data applying intraoperative imaging and navigation (study no. 99/18).

Preoperative imaging and image processing

Tumors were segmented manually in preoperative magnetic resonance imaging (MRI) data applying the smart brush element (Brainlab, Munich, Germany). Additionally, in selected cases, vascular structures were segmented based on time of flight MRI and computed tomography (CT) angiography examinations. Preoperative CT images were used for automatic vertebra segmentation, providing individual vertebra objects with an automatic color assignment (anatomical mapping element, Brainlab). Auto-segmentation results were fine-tuned applying the smart brush element before the CT and MRI were fused. In case that rigid registration showed a deviation in the area of interest due to the flexibility of the spine, non-linear registration was additionally applied; in these cases, the linear registration was used as an initial approximation for the non-linear registration (spine curvature correction element, Brainlab). The segmented outlines of the vertebra, which could be visualized in all fused datasets were used to verify the final registration result.

Intraoperative registration scanning

All patients were placed in prone position on the OR table of a 32-slice CT scanner (AIRO, Brainlab). Details of the setting were described previously [7]. In the cases of a tumor in the upper cervical spine (case no. 1, 2, 5, 7, 8, 10), the head was fixed with a carbon fiber head holder and the navigation reference array was attached to the head holder. In the other cases, the reference array was firmly taped on the patient's skin after draping caudal to the skin incision. Intraoperative registration scanning was performed after approaching the spine, retractor placement, and laminectomy to avoid a shifting of structures due to the approach procedure. Registration scanning was performed applying low-dose protocols. The effective dose (ED) of intraoperative CT (iCT) for registration scanning was determined by multiplying the dose length product by 5.4 μSv/Gy*cm for cervical and 17.8 μSv/Gy*cm for thoracic scans referring to phantoms with a diameter of 16 cm and 32 cm respectively. Accuracy of automatic patient registration was monitored by measuring the offset of skin fiducials, which were not part of the registration process, so that a target registration error (TRE) could be calculated.

AR

The preoperative images including the segmented objects, that should be visualized by AR, were registered non-linearly with the low-dose CT scan, which was the reference for patient registration, i.e., defining the navigation coordinate system.

AR was established as "see-through" AR applying the HUD of the operating microscopes Pentero and Pentero900 (Zeiss, Oberkochen, Germany) in conjunction with the microscope element software (Brainlab) providing an additional AR

Table 1 patient characteristics

No.	Age (yrs.)	Sex	Diagnosis	Level	Procedure
1	65	f	Meningioma WHO I	C2–C3	Laminectomy C2–C3, complete resection
2	59	m	Squamous cell lung carcinomametastasis	C0–C3	Craniotomy posterior fossa and laminectomy C1–C3, resection of intradural tumor
3	66	m	Meningioma WHO I	T7	Laminectomy T6–T8, complete resection
4	84	f	Meningioma WHO I	T1–T2	Laminectomy T1–T2, complete resection
5	57	f	Meningioma WHO I	C1	Laminectomy C1, complete resection
6	76	f	Meningioma WHO I	T11–T12	Laminectomy T11–T12 complete resection
7	66	f	Meningioma WHO I	C1	Laminectomy C1, complete resection
8	59	m	Glioma WHO II	C0–C3	Craniotomy posterior fossa and laminectomy C1, biopsy
9	38	f	Ependymoma WHO II	C7–T2	Laminectomy C7–T2, complete resection
10	36	f	Hemangioblastoma WHO I	C1	Laminectomy C1, complete resection

f female, *m* male, *WHO* World Health Organization, *yrs*. years

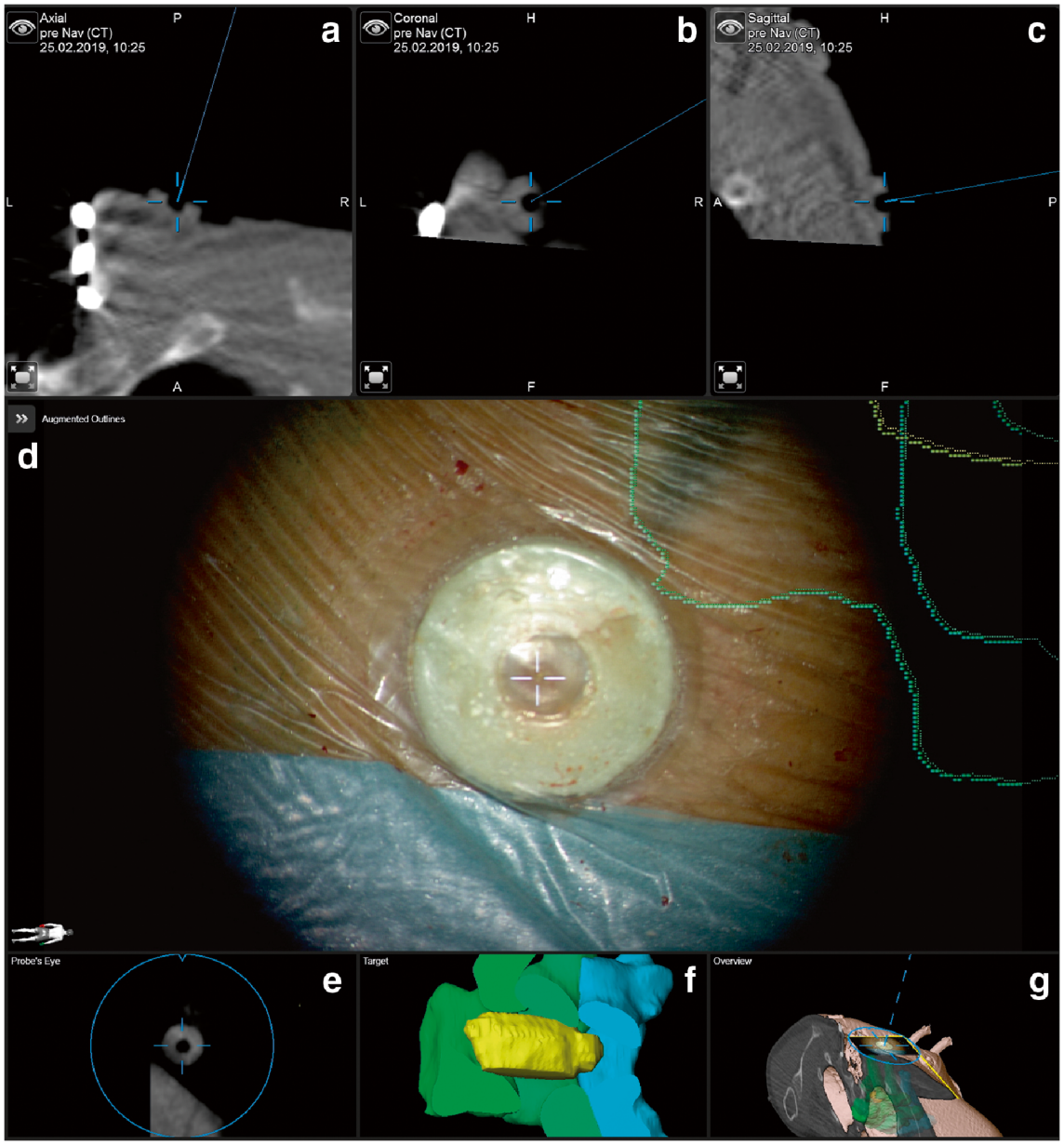

Fig. 1 The overall AR accuracy is checked by focusing with the operating microscope in the divots of the skin fiducials (case no. 9) (A, axial; B, coronal; C, sagittal view of iCT images; D, AR visualization focusing in the center of the skin fiducial; E, probe's eye view of iCT images; F, target view visualizing the displayed AR objects; G, 3D rendering of the iCT images illustrating how the video frame is placed relative to the image data)

visualization on screens close to the surgical site, as "video-pass-through" AR. This allowed visualization of AR independent of the HUD in parallel to other forms of visualization with solid three-dimensional (3D) objects, transparent object display, an overview display visualizing how the viewing frame relates to the 3D image data, and standard navigational displays depicting different kinds of image data reformatted in standard axial, coronal, sagittal, inline, and probe's eye views, as well as additional 3D renderings. AR microscope calibration was performed by identification of several markers on the reference array and if necessary, adjusting the 3D AR outline of the registration array. Overall AR accuracy was maintained by identifying objects in the surgical field such as retractors and other artificial landmarks such as the skin fiducials, which were used to calculate the TRE.

AR was available in two different principal visualization forms, either each AR object was visualized as a combination of solid and dotted lines, in which the solid line represents the extent of the object in the focus plane and the dotted line the maximum extent beyond the focus plane in the depth, or the objects were displayed in a 3D fashion as semitransparent objects with contours giving a representation of the 3D shape

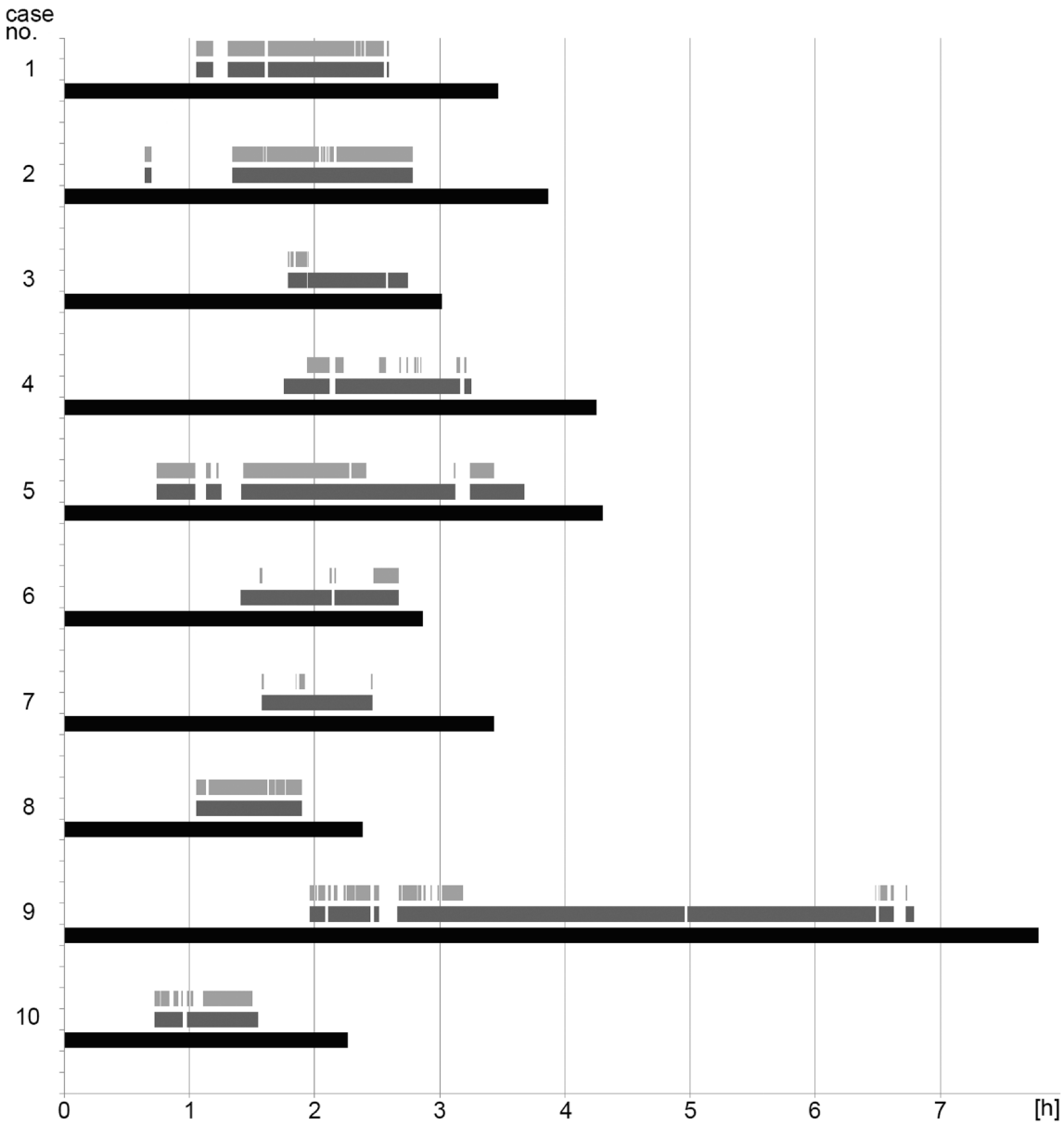

Fig. 2 AR usage in all 10 patients; black bars represent the total surgery time (skin incision to skin closure), dark gray bars the microscope usage time, and light bars the time the HUD was switched on and AR was visualized directly in the viewing field of the operating microscope

in space. Each object could be switched on or off individually. AR usage was evaluated by analyzing the microscope video documentation. The instances when AR was switched off were counted, as well as the time segments were measured. Interruption of the microscope usage, which in most of the cases, was mainly due to the application of intraoperative ultrasound, which was not part of this study, and was not counted as interruption of AR usage.

Results

AR could be integrated into the surgical workflow for intradural tumor surgery without problems. Automatic registration based on iCT scanning resulted in a registration accuracy measured as TRE of 0.72 ± 0.24 mm (mean ± standard deviation), with a minimum of 0.49 mm and a maximum of 1.10 mm. The overall AR accuracy was repeatedly ensured during the procedure by focusing into the center of the skin fiducials with the operating microscope (Fig. 1), as well as checking the close overlay of the AR representation of the reference array and reality.

The total ED for the low-dose registration iCT including the scout scan ranged for the cervical region from 0.09–0.53 mSv (mean ± standard deviation 0.22 ± 0.16 mSv) and for the thoracic region from 0.93–2.30 mSv (mean ± standard deviation 1.68 ± 0.61 mSv). In 4 cases (2, 4, 8, and 10), we could omit the scout scan further decreasing the total ED. The

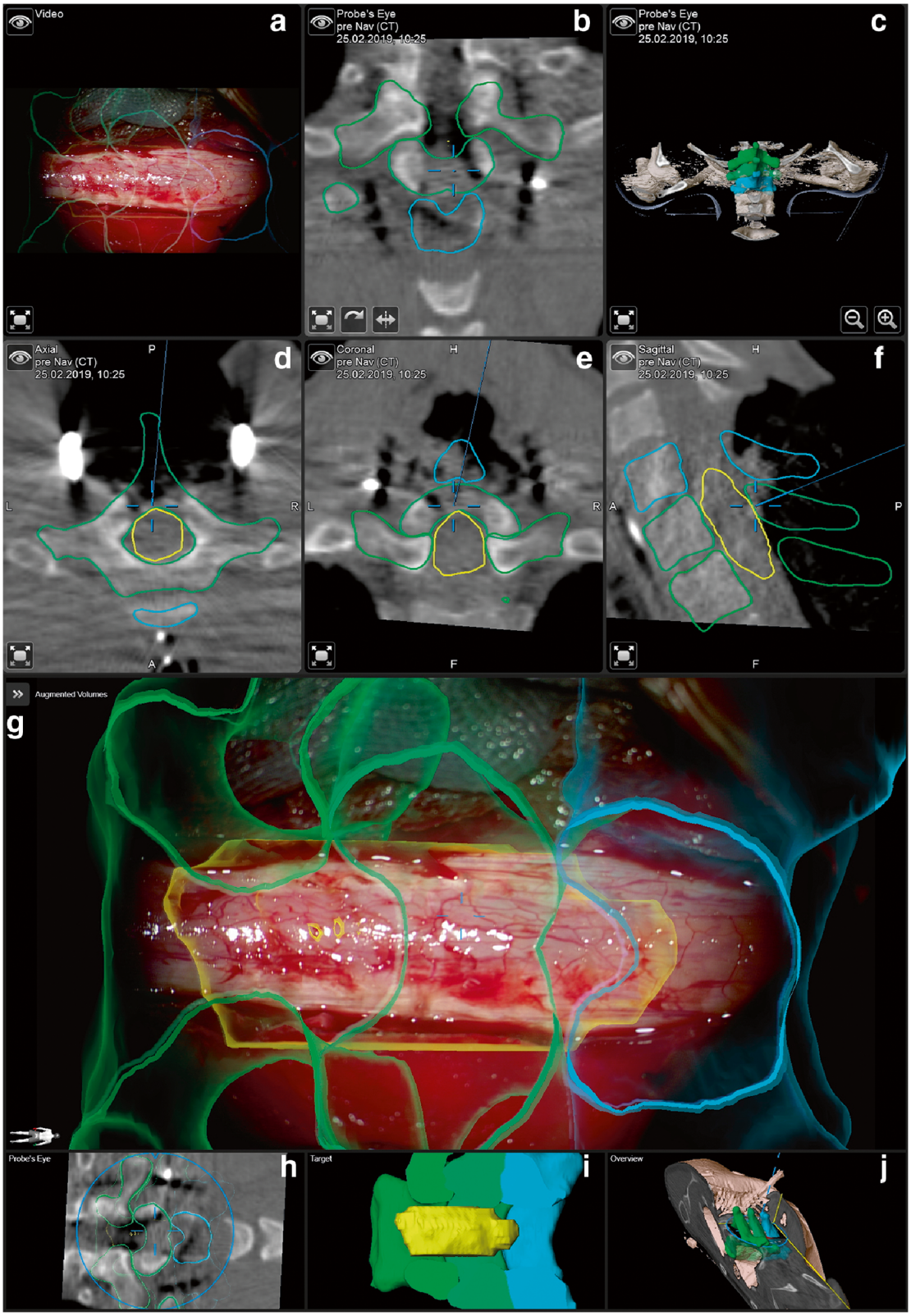

Fig. 3 Thirty-eight-year-old female patient with an ependymoma C7 - T2 (case no. 9), 4 objects were visualized by AR (yellow: tumor, blue: vertebra C7, green shades: vertebra T1 and T2) (A, microscope video; B, probe's eye view; C, 3D probe's eye view; D, axial; E, coronal; F, sagittal view of iCT registration scan; G, AR visualization prior to dural opening; H, probe's eye view, with a blue circle depicting the viewing field of the operating microscope; I, target view visualizing the displayed AR objects; J, 3D rendering of the iCT images illustrating how the video frame is placed in relation to the image data)

scan length of the scout scan was in the range of 101–165 mm (mean ± standard deviation 132 ± 24 mm) in 6 patients and the scan length of the helical scan ranged from 60 to 120 mm (mean ± standard deviation 85.3 ± 23.5 mm).

AR reliably visualized the structures of interest in the surgical field. We observed a very close matching of the visualized objects and the visible tumor outline. The microscope AR visualization allowed a good hand-eye coordination analog to microscope-based AR for cranial applications. To avoid an information overflow, individual objects could be switched off, so that e.g., only the tumor object was visualized during the resection of the tumor, while the objects visualizing the surrounding structures, such as vertebral bodies and vascular structures, were visualized often only prior to dural opening and at the beginning of the resection. AR usage varied greatly between the different cases (Fig. 2). The total microscope time ranged from 48 to 269 min (mean ± standard deviation 96 ± 68 min); the overall AR time, i.e., the time the HUD was switched on and AR, was visualized in the direct microscope view ranged from 5 to 92 min (mean ± standard deviation 45 ± 32 min). The microscope AR usage in relation to the total microscope time ranged from 9.0–97.9% (mean ± standard deviation 51.6 ± 36.7%). Counting the incidence of how often the HUD was switched off during microscope usage resulted in a range of 2 to 17 times per surgical case (mean ± standard deviation 5.7 ± 4.4 times). Independent of the status of microscope AR visibility the AR overlay was visualized on nearby monitors over the entire microscope time.

The 3D display of AR objects provided an intuitive depth perception; however, in intradural tumor surgery, this depth perception was of minor importance due to the limited size of the tumors in depth extent. AR gave a good impression about the extent of the tumor especially in probe's eye projection in general which proved to be especially helpful in the case of an intramedullary ependymoma (Figs. 3 and 4), where the outlines were very useful to visualize the cranio-caudal tumor extent. Nevertheless, in this particular case, AR was switched off over longer periods of resection since the microscope viewing field was sometimes so enlarged that the tumor contours were outside the viewing field or the AR object outlines blurred identifying the interface of normal medulla and ependymoma. In these instances, the solid/dotted line AR representation often provided a good compromise between obscured view and switching off the microscope HUD, which is demonstrated in another intramedullary tumor, a hemangioblastoma. Figure 5 illustrates the close matching of the visible extent of the tumor and the AR display and Fig. 6 provides a direct comparison between 3D and solid/dotted line AR visualization. An example how risk structures such as vascular structures can be visualized by AR is depicted in the case of a C1 meningioma in Figs. 7 and 8. AR not only shows a precise matching with reality but also provides a very good impression on the individual patient anatomy beyond the immediate microsurgical exposure, thereby facilitating orientation (Fig. 8A).

Discussion

Up to now, most approaches to implement AR for spine procedures were based on visualizing systems displaying AR on monitors applying optical cameras [3, 11] or optical see-through head mounted devices (HMDs), like in setups guiding pedicle screw placements [15, 22, 26, 36] or percutaneous procedures like vertebroplasties [1, 10], and facet joint injections [2]. After first attempts to transfer the technique of microscope-based AR using the HUDs of operating microscopes from cranial neurosurgical applications to spine surgery were successful [20, 35], we had implemented AR support for spine surgery using commercially available system components [7]. To our knowledge, this is the first report on a prospective series of intradural spinal tumors operated with AR support.

Microscope-based AR was smoothly integrated in the surgical workflow, so that it can be routinely used. In all cases, we could observe a very close matching of the visible extent of the tumor and its AR representation. AR provided an intuitive visualization of the overall extent of the tumor and its surrounding structures. Since AR was visualized using the microscope HUD, there was a smooth hand-eye coordination and no parallax problem [25]. The depth perception was improved by the 3D shaped display of the segmented objects, which however sometimes blurred the clear perception of the surgical field, so that the AR display could be altered to a line-mode display visualizing the extent of the tumor as closed lines in the focal plane and the maximum extent beyond the focal plane as dotted lines, similar to the historic initial visualization mode of AR in cranial microscope-based AR (for comparison see Fig. 6). An information overflow or crowding of the surgical viewing field by AR objects could be avoided by the possibility to selectively switch on and off each object. It is essential that only the objects of importance for the specific surgical step are visualized to avoid disturbing the surgeon [25]. Analyzing the microscope HUD AR usage time showed a great variability. On average 51.6% of overall microscope usage the microscope HUD was switched on with a range of 9.0–97.9%. In parallel, the AR visualization was displayed on screens close to the surgical field for the whole microscope usage time independent of the status of microscope HUD AR. The microscope HUD was switched off during microscope usage on an average of 5.7 times per surgical case with a range of 2 to 17 times. This demonstrates that the AR representation in the direct surgical microscope view is not yet optimal and sometimes obscures the clear view. A better contrast adaptation and resolution of the HUD have to be developed, as well as the AR visualization itself has to

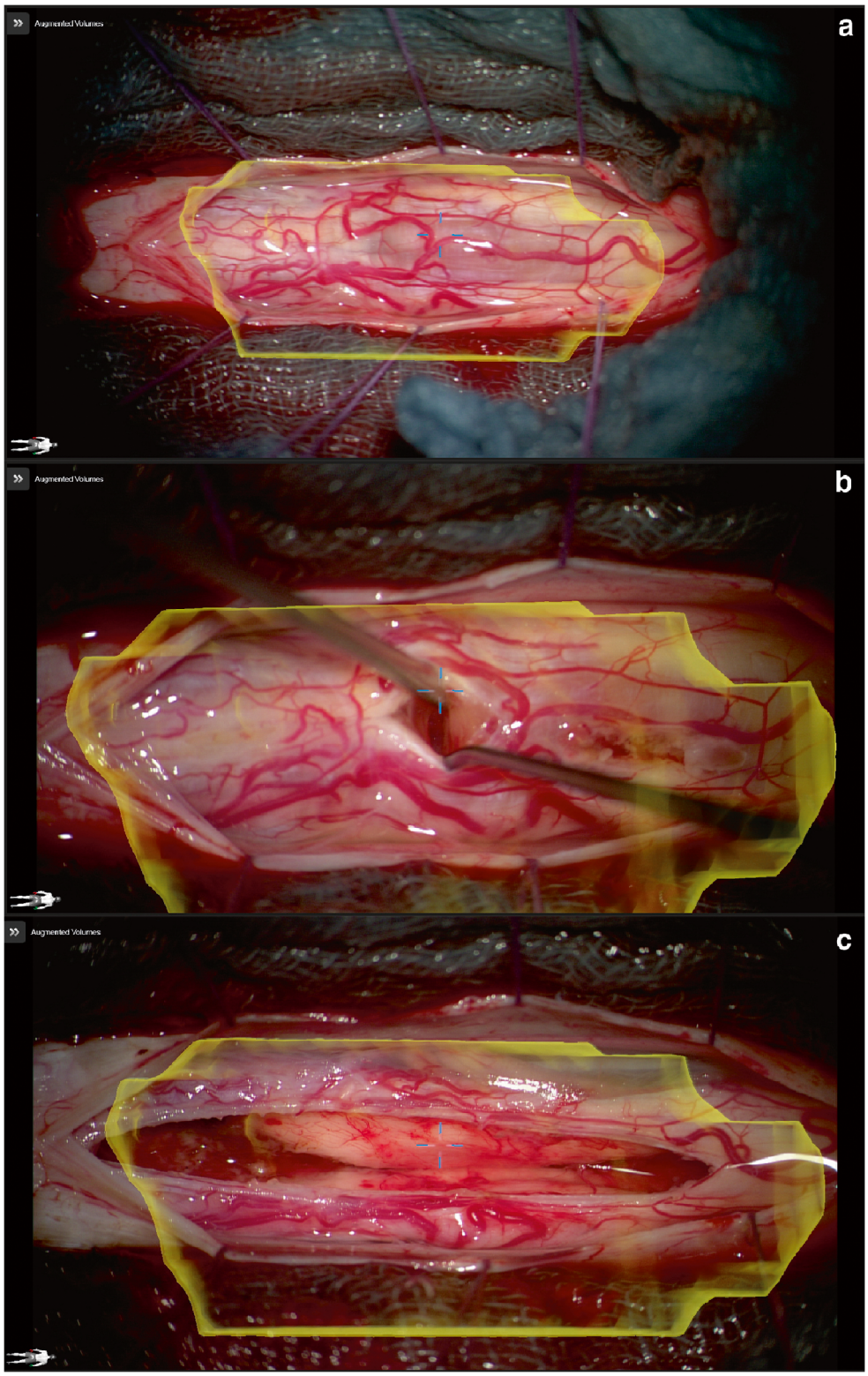

Fig. 4 Same patient as in Fig. 3, microscope-based AR visualizing the tumor outline (A, immediately after dural opening; B, at the beginning of resection; C, at the end of resection)

become even more immersive in order to avoid that the AR visualization is perceived as it is solely projected on top of reality. Furthermore, aspects of mixed reality have to be integrated, in which the visualized objects actually can interact with reality.

Automatic registration applying iCT resulted in a very low registration error of 0.72 ± 0.24 mm, which corresponds very well to a recent spine phantom study showing a significant benefit of intraoperative imaging-based automatic registration in comparison to point-to-point registration with

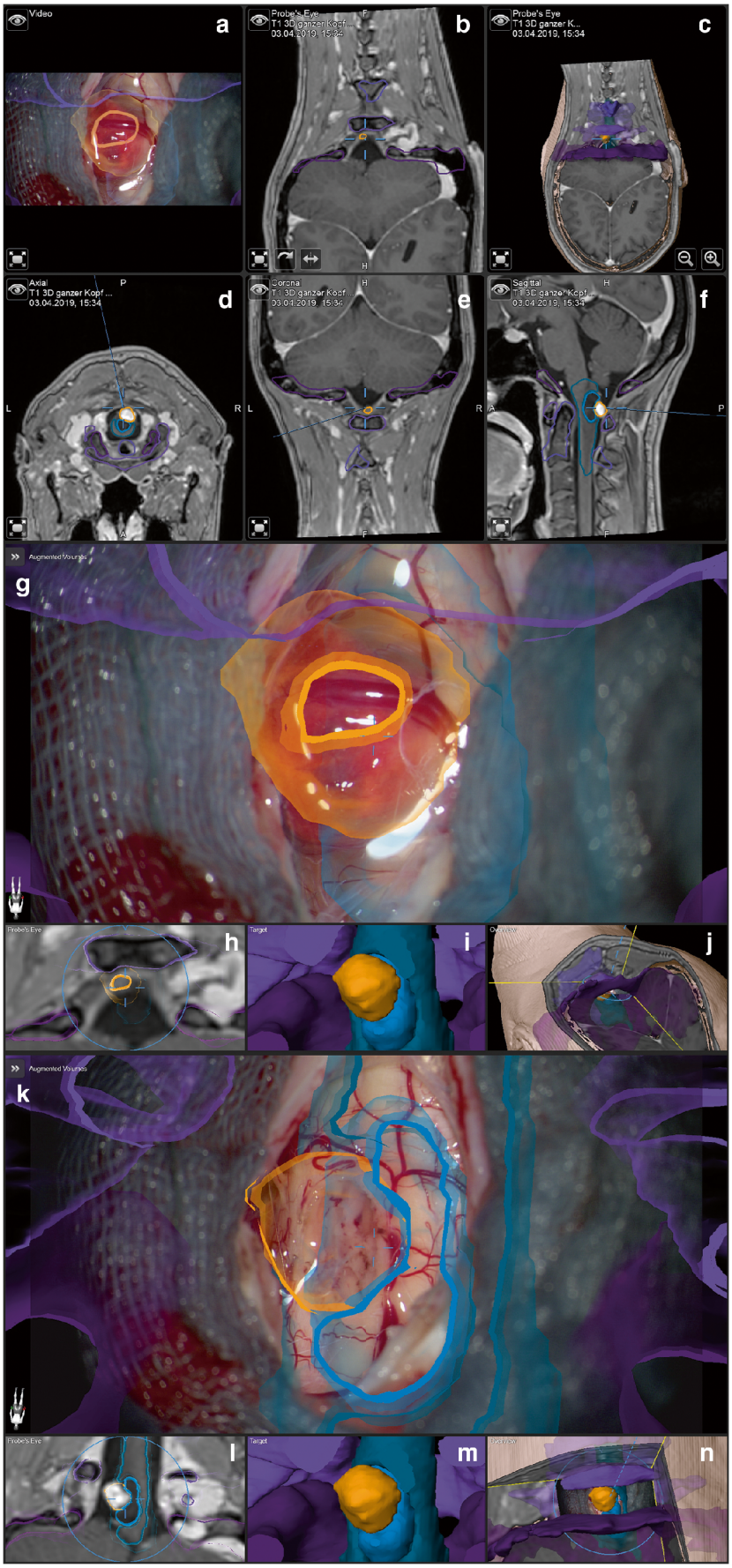

Fig. 5 Thirty-six-year-old female patient with a hemangioblastoma C1 (case no. 10), 5 objects were visualized by AR (yellow: solid contrast enhancing tumor, blue: tumor cyst, shades of violet: C0, C1, and C2) (A, microscope video; B, probe's eye view; C, 3D probe's eye view; D, axial; E, coronal; F, sagittal view of T1-weighted post contrast 3D MRI; G, AR visualization after laminectomy of C1 and dural opening; H, probe's eye view, with a blue circle depicting the viewing field of the operating microscope; I, target view visualizing the displayed AR objects; J, 3D rendering of the T1-weighted MRI illustrating how the video frame is placed in relation to the image data; K/L/M/N, correspond to G/H/I/J after resection of the tumor)

registration errors of 0.74 ± 0.30 mm and 1.10 ± 0.61 mm respectively [37]. Automatic iCT-based registration is to date the most robust and reliable strategy to ensure high registration accuracy. Applying low-dose protocols and minimizing the scan length allowed to decrease the radiation exposure to an ED with a mean of 0.22 mSv for cervical and 1.68 mSv for thoracic procedures. This can be compared to an ED of about 3 mSv an average person in the USA receives per year from natural radiation. When applying low-dose scanning to reduce ED, it is important that the success of the procedure is not compromised [16, 33, 34]. In regard to AR accuracy, even a further reduction of the ED might be possible to the point when image artifacts and low image resolution prevent a reliable registration with the preoperative image data. Radiation free registration methods like surface matching and point-to-point registration [37] using a pointer or settings using ultrasound to delineate the shape of the bony structures of the spine for registration [23] are no realistic alternatives since they are much more inaccurate than automatic iCT-based registration.

Maintaining accuracy of AR during spinal surgery has the same challenges as in cranial procedures and navigation per se. There are potential inaccuracies during the course of surgery that might be caused by positional shifting. This occurs either by a movement of the coordinate system, i.e., a movement of the reference array in relation to the surgical field, or by a change of the integrity of the bony structures of the spine caused by resection or simple acting forces changing the relative alignment and geometry of the vertebra. Therefore, repeated landmark checks and the application of clearly identifiable artificial landmarks are mandatory. If positional shifting occurs, repeated low-dose registration scanning provides a possibility to restore AR registration accuracy. Furthermore, effects well known as brain shift in cranial navigation [28] might also occur in intradural spinal tumor surgery, caused by a movement of the spinal cord due to decompression and cerebrospinal fluid loss, as well as changes in tumor shape due to resection.

In surgery for intradural tumors, the use of the operating microscope is at the moment still the primary device for

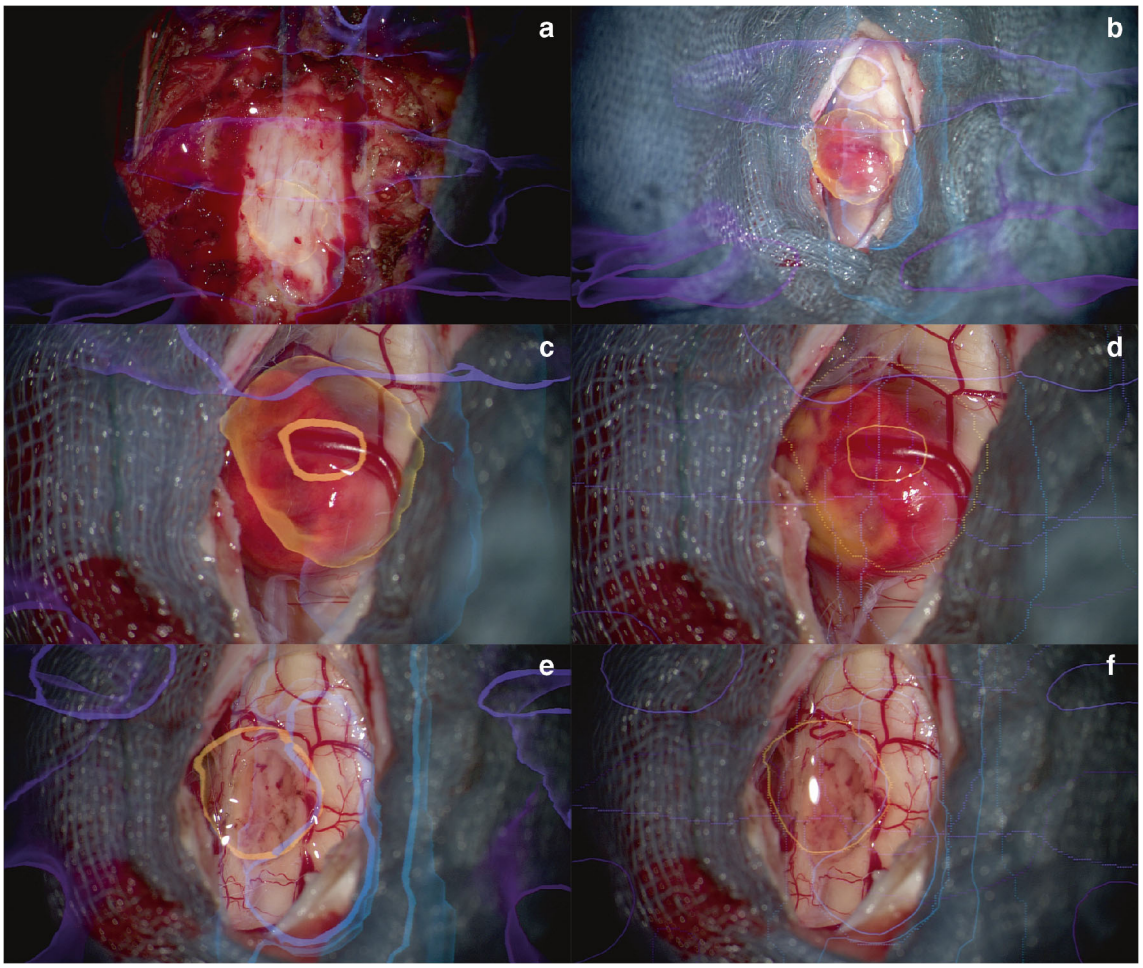

Fig. 6 Same patient as in Fig. 5 depicting the AR visualization in the course of surgery (A, after laminectomy of C1 and prior to dural opening; B, after dural opening; C/D, before; E/F, after resection of the tumor); C/D and E/F show the same situation with an AR visualization depicting 3D objects (C/E) or the solid/dotted line representations of the AR objects (D/F)

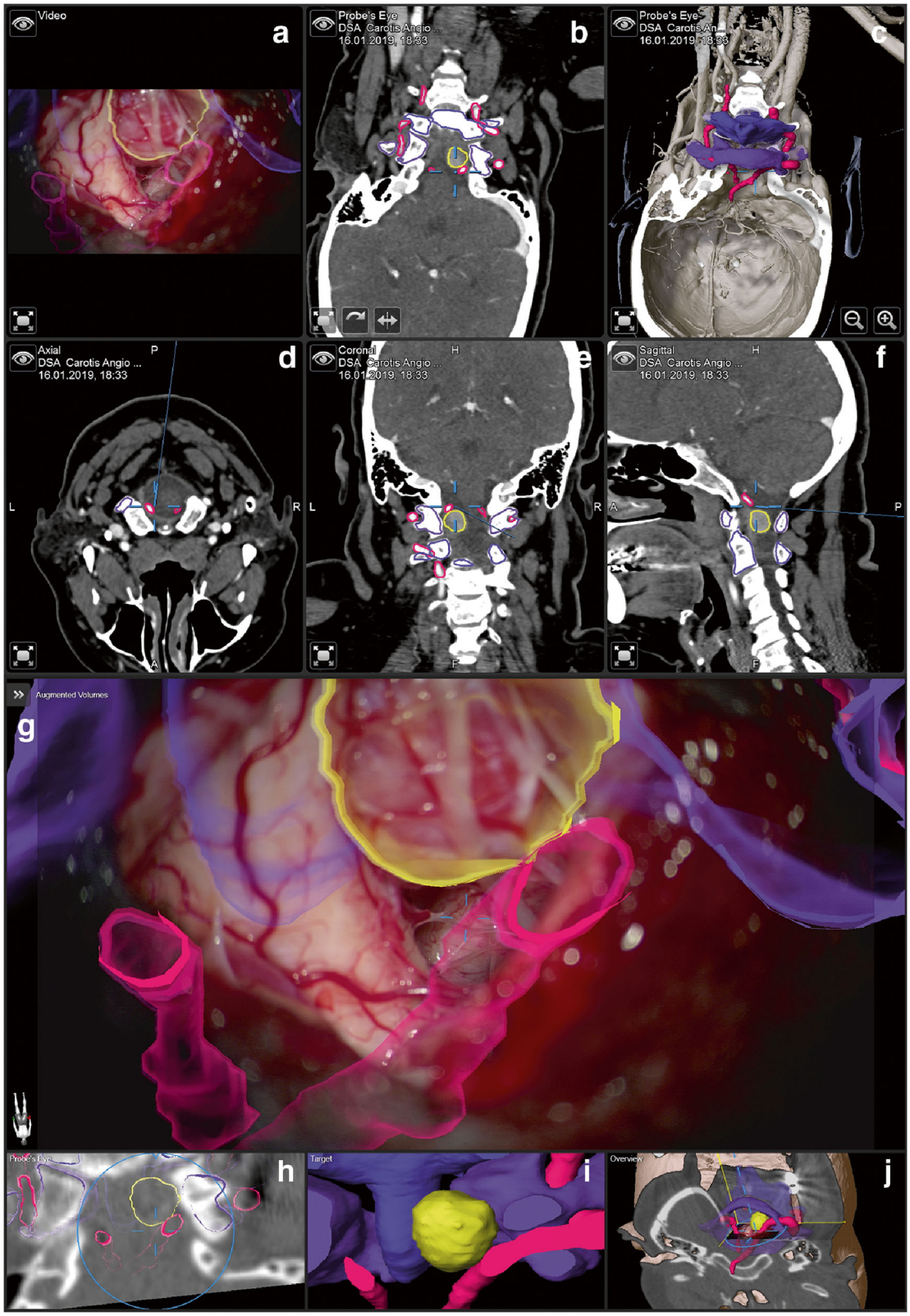

Fig. 7 Sixty-six-year-old female patient with a meningioma C1 (case no. 7)), 4 objects were visualized by AR (yellow: tumor, red: course of vertebral arteries, shades of violet: C0, C1) (A, microscope video; B, probe's eye view; C, 3D probe's eye view; D, axial; E, coronal; F, sagittal view of CT angiography; G, AR visualization after laminectomy of C1 and dural opening, the blue cross of the center of the microscope viewing field is focused on the medial wall of the left vertebral artery; H, probe's eye view, with a blue circle depicting the viewing field of the operating microscope; I, target view visualizing the displayed AR objects; J, 3D rendering of the iCT images illustrating how the video frame is placed in relation to the image data)

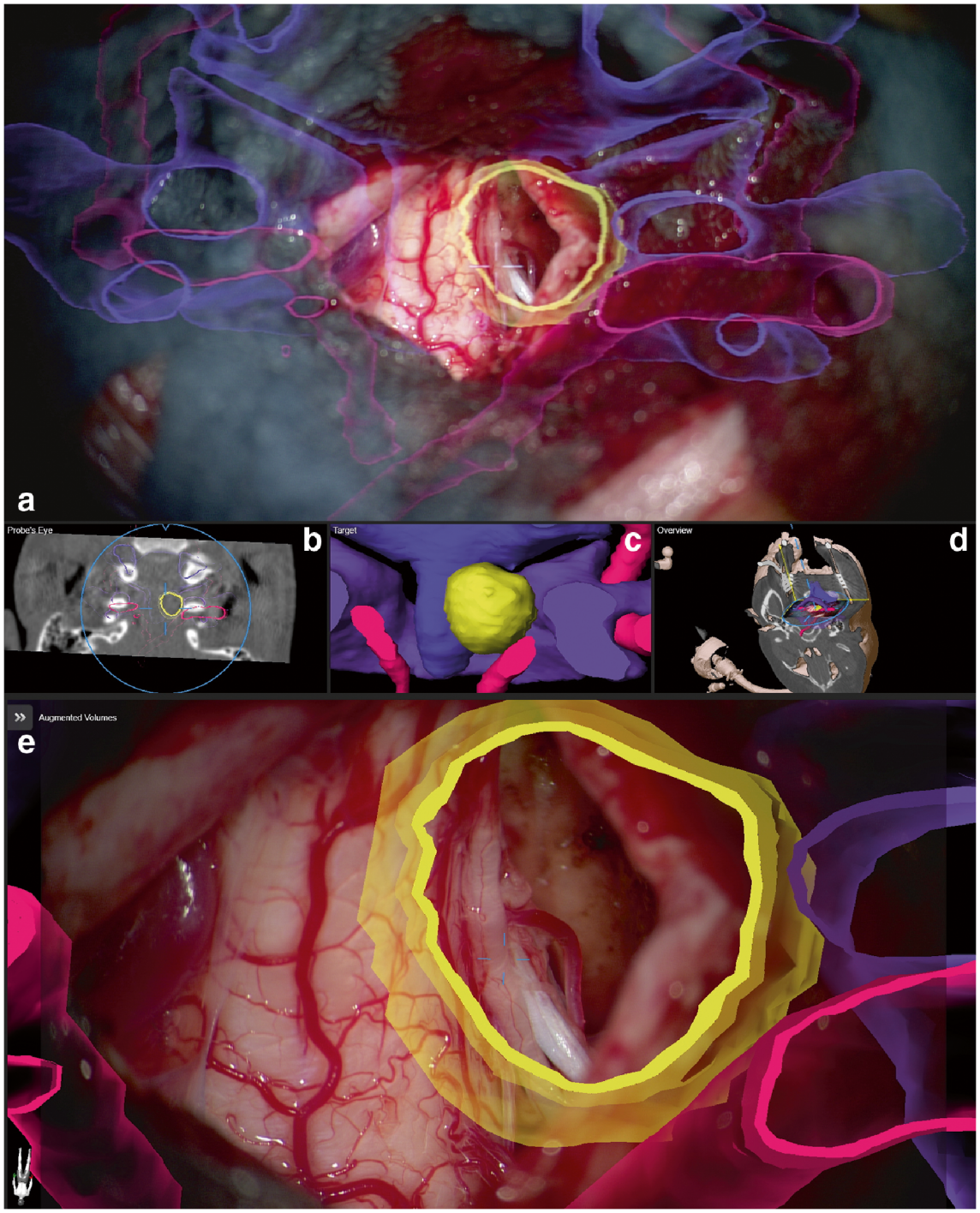

Fig. 8 Same patient as in Fig. 7 depicting the situation at the end of resection (A, microscope video showing the AR visualization of the C1 and C2 vertebra, the course of the vertebral arteries, as well as the tumor outline; B, probe's eye view, with a blue circle depicting the viewing field of the operating microscope; C, target view visualizing the displayed AR objects; D, 3D rendering of the iCT images illustrating how the video frame is placed in relation to the image data; E, enlarged AR view

optimal visualization, so that AR techniques based on HMDs will be preferably used in cases where no operating microscope is needed like, e.g., in pedicle screw placements and percutaneous procedures. Exoscopes might become an alternative to standard operating microscopes and also find their way into spine surgery [21]. Straightforward integration of AR in such systems is possible, as demonstrated for open liver surgery [13, 31].

Limitations of our prospective observational study are the small number of cases and the difficulty to prove that AR actually impacted the course of surgery, as well as to prove that AR might even result in better clinical outcomes. AR

support in spine surgery might be felt as unnecessary or as technical overtreatment in easy clinical cases. In cases in which the tumor is easily seen at the surface of the spinal cord, or e.g., the extent of a meningioma is clearly visible after dural opening, AR at first sight provides only marginal additional information; however, these cases provide a very good possibility to check the accuracy and reliability of the overall AR implementation, so that it has been proven reliable when used in complicated cases, in which there is an invisible extension of a tumor below other structures which can be well visualized by AR. The same applies for surrounding structures that might be important to be preserved, like vascular structures. Intraoperative real-time imaging, i.e., intraoperative ultrasound, is a potential alternative to delineate the extent of an intramedullary tumor. Combining AR and intraoperative ultrasound might provide a possibility to correct for registration inaccuracies, as well as surgically induced changes in position and shape of structures, like navigation updating by intraoperative imaging and compensation for brain shift [28].

Microscope-based AR for spinal surgery is integrated into the same framework as microscope-based AR for cranial applications. Therefore, this setting is open to integrate all kinds of different imaging modalities like in multimodal cranial navigation [14, 29, 30] and provides the possibility of multimodal spinal AR. Besides the immediate effect of supporting the surgeon during the actual procedure, spinal AR has a huge potential in resident education [9].

Conclusions

Microscope-based AR can be successfully applied to intradural spine tumor surgery providing an intuitive intraoperative visualization of the tumor extent and surrounding structures. Automatic low-dose intraoperative computed tomography registration ensures high accuracy. Thus, all advanced multi-modality options of cranial AR can now also be applied to spinal surgery.

Acknowledgments We thank J.-W. Bartsch for proofreading the manuscript.

Compliance with ethical standards

Conflict of interest All authors certify that they have no affiliations with or involvement in any organization or entity with any financial interest (such as honoraria; educational grants; participation in speakers' bureaus; membership, employment, consultancies, stock ownership, or other equity interest; and expert testimony or patent-licensing arrangements) or non-financial interest (such as personal or professional relationships, affiliations, knowledge, or beliefs) in the subject matter or materials discussed in this manuscript, except that B. Carl and Ch. Nimsky have received speaker fees from Brainlab.

Ethical standards All procedures performed were in accordance with the ethical standards of the institutional and/or national research committee and with the 1964 Helsinki Declaration and its later amendments or comparable ethical standards. We obtained ethics approval for prospective archiving clinical and technical data applying intraoperative imaging and navigation (study no. 99/18). Informed consent was obtained from all individual participants included in the study.

References

1. Abe Y, Sato S, Kato K, Hyakumachi T, Yanagibashi Y, Ito M, Abumi K (2013) A novel 3D guidance system using augmented reality for percutaneous vertebroplasty: technical note. J Neurosurg Spine 19:492–501. https://doi.org/10.3171/2013.7.SPINE12917
2. Agten CA, Dennler C, Rosskopf AB, Jaberg L, Pfirrmann CWA, Farshad M (2018) Augmented reality-guided lumbar facet joint injections. Investig Radiol 53:495–498. https://doi.org/10.1097/RLI.0000000000000478
3. Burstrom G, Nachabe R, Persson O, Edstrom E, Terander AE (2019) Augmented and virtual reality instrument tracking for minimally invasive spine surgery: a feasibility and accuracy study. Spine (Phila Pa 1976). https://doi.org/10.1097/BRS.0000000000003006
4. Cabrilo I, Bijlenga P, Schaller K (2014) Augmented reality in the surgery of cerebral arteriovenous malformations: technique assessment and considerations. Acta Neurochir 156:1769–1774. https://doi.org/10.1007/s00701-014-2183-9
5. Cabrilo I, Sarrafzadeh A, Bijlenga P, Landis BN, Schaller K (2014) Augmented reality-assisted skull base surgery. Neurochirurgie 60:304–306. https://doi.org/10.1016/j.neuchi.2014.07.001
6. Carl B, Bopp M, Chehab S, Bien S, Nimsky C (2018) Preoperative 3-dimensional angiography data and intraoperative real-time vascular data integrated in microscope-based navigation by automatic patient registration applying intraoperative computed tomography. World Neurosurg 113:E414–E425. https://doi.org/10.1016/j.wneu.2018.02.045
7. Carl B, Bopp M, Sass B, Voellger B, Nimsky C (2019) Implementation of augmented reality support in spine surgery. Eur Spine J. https://doi.org/10.1007/s00586-019-05969-4
8. Carl B, Bopp M, Voellger B, Sass B, Nimsky C (2019) Augmented reality in transsphenoidal surgery. World Neurosurg 125:E873–E883. https://doi.org/10.1016/j.wneu.2019.01.202
9. Coelho G, Defino HLA (2018) The role of mixed reality simulation for surgical training in spine: phase 1 validation. Spine (Phila Pa 1976) 43:1609–1616. https://doi.org/10.1097/BRS.0000000000002856
10. Deib G, Johnson A, Unberath M, Yu K, Andress S, Qian L, Osgood G, Navab N, Hui F, Gailloud P (2018) Image guided percutaneous spine procedures using an optical see-through head mounted display: proof of concept and rationale. J Neurointerv Surg 10:1187–1191. https://doi.org/10.1136/neurintsurg-2017-013649
11. Elmi-Terander A, Burstrom G, Nachabe R, Skulason H, Pedersen K, Fagerlund M, Stahl F, Charalampidis A, Soderman M, Holmin S, Babic D, Jenniskens I, Edstrom E, Gerdhem P (2019) Pedicle screw placement using augmented reality surgical navigation with intraoperative 3D imaging: a first in-human prospective cohort study. Spine (Phila Pa 1976) 44:517–525. https://doi.org/10.1097/BRS.0000000000002876
12. Fahlbusch R, Nimsky C, Ganslandt O, Steinmeier R, Buchfelder M, Huk W (1998) The Erlangen concept of image guided surgery. In: Lemke HU, Vannier MW, Inamura K, Farman A (eds) CAR'98. Elsevier Science B.V., Amsterdam, pp 583–588

13. Fida B, Cutolo F, di Franco G, Ferrari M, Ferrari V (2018) Augmented reality in open surgery. Updat Surg 70:389–400. https://doi.org/10.1007/s13304-018-0567-8
14. Ganslandt O, Stadlbauer A, Fahlbusch R, Kamada K, Buslei R, Blumcke I, Moser E, Nimsky C (2005) Proton magnetic resonance spectroscopic imaging integrated into image-guided surgery: correlation to standard magnetic resonance imaging and tumor cell density. Neurosurgery 56:291. https://doi.org/10.1227/01.NEU.0000156782.14538.78
15. Gibby JT, Swenson SA, Cvetko S, Rao R, Javan R (2019) Head-mounted display augmented reality to guide pedicle screw placement utilizing computed tomography. Int J Comput Assist Radiol Surg 14:525–535. https://doi.org/10.1007/s11548-018-1814-7
16. Greffier J, Pereira FR, Viala P, Macri F, Beregi JP, Larbi A (2017) Interventional spine procedures under CT guidance: how to reduce patient radiation dose without compromising the successful outcome of the procedure? Phys Med 35:88–96. https://doi.org/10.1016/j.ejmp.2017.02.016
17. Kelly PJ, Alker GJ Jr, Goerss S (1982) Computer-assisted stereotactic microsurgery for the treatment of intracranial neoplasms. Neurosurgery 10:324–331
18. King AP, Edwards PJ, Maurer CR, de Cunha DA, Hawkes DJ, Hill DLG, Gaston RP, Fenlon MR (1999) A system for microscope-assisted guided interventions. Stereotact Funct Neurosurg 72:107–111. https://doi.org/10.1159/000029708
19. Kiya N, Dureza C, Fukushima T, Maroon JC (1997) Computer navigational microscope for minimally invasive neurosurgery. Minim Invasive Neurosurg 40:110–115. https://doi.org/10.1055/s-2008-1053429
20. Kosterhon M, Gutenberg A, Kantelhardt SR, Archavlis E, Giese A (2017) Navigation and image injection for control of bone removal and osteotomy planes in spine surgery. Oper Neurosurg (Hagerstown) 13:297–304. https://doi.org/10.1093/ons/opw017
21. Kwan K, Schneider JR, Du V, Falting L, Boockvar JA, Oren J, Levine M, Langer DJ (2019) Lessons learned using a high-definition 3-dimensional exoscope for spinal surgery. Oper Neurosurg (Hagerstown) 16:619–625. https://doi.org/10.1093/ons/opy196
22. Liebmann F, Roner S, von Atzigen M, Scaramuzza D, Sutter R, Snedeker J, Farshad M, Furnstahl P (2019) Pedicle screw navigation using surface digitization on the Microsoft HoloLens. Int J Comput Assist Radiol Surg 14:1157–1165. https://doi.org/10.1007/s11548-019-01973-7
23. Ma L, Zhao Z, Chen F, Zhang B, Fu L, Liao H (2017) Augmented reality surgical navigation with ultrasound-assisted registration for pedicle screw placement: a pilot study. Int J Comput Assist Radiol Surg 12:2205–2215. https://doi.org/10.1007/s11548-017-1652-z
24. Mascitelli JR, Bederson JB (2018) In reply: navigation-linked heads-up display in intracranial surgery: early experience. Oper Neurosurg (Hagerstown) 14:E73. https://doi.org/10.1093/ons/opy049
25. Meola A, Cutolo F, Carbone M, Cagnazzo F, Ferrari M, Ferrari V (2017) Augmented reality in neurosurgery: a systematic review. Neurosurg Rev 40:537–548. https://doi.org/10.1007/s10143-016-0732-9
26. Molina CA, Theodore N, Ahmed AK, Westbroek EM, Mirovsky Y, Harel R, Orru E, Khan M, Witham T, Sciubba DM (2019) Augmented reality-assisted pedicle screw insertion: a cadaveric proof-of-concept study. J Neurosurg Spine:1–8. https://doi.org/10.3171/2018.12.SPINE181142
27. Nakamura M, Tamaki N, Tamura S, Yamashita H, Hara Y, Ehara K (2000) Image-guided microsurgery with the Mehrkoordinaten manipulator system for cerebral arteriovenous malformations. J Clin Neurosci 7(Suppl 1):10–13. https://doi.org/10.1054/jocn.2000.0702
28. Nimsky C, Ganslandt O, Cerny S, Hastreiter P, Greiner G, Fahlbusch R (2000) Quantification of, visualization of, and compensation for brain shift using intraoperative magnetic resonance imaging. Neurosurgery 47:1070–1079. https://doi.org/10.1097/00006123-200011000-00008
29. Nimsky C, Ganslandt O, Fahlbusch R (2006) Implementation of fiber tract navigation. Neurosurgery 58:292–303. https://doi.org/10.1227/01.NEU.0000204726.00088.6D
30. Nimsky C, Ganslandt O, Kober H, Moller M, Ulmer S, Tomandl B, Fahlbusch R (1999) Integration of functional magnetic resonance imaging supported by magnetoencephalography in functional neuronavigation. Neurosurgery 44:1249–1255. https://doi.org/10.1097/00006123-199906000-00044
31. Ntourakis D, Memeo R, Soler L, Marescaux J, Mutter D, Pessaux P (2016) Augmented reality guidance for the resection of missing colorectal liver metastases: an initial experience. World J Surg 40:419–426. https://doi.org/10.1007/s00268-015-3229-8
32. Roberts DW, Strohbehn JW, Hatch JF, Murray W, Kettenberger H (1986) A frameless stereotaxic integration of computerized tomographic imaging and the operating microscope. J Neurosurg 65:545–549. https://doi.org/10.3171/jns.1986.65.4.0545
33. Sarwahi V, Payares M, Wendolowski S, Maguire K, Thornhill B, Lo YT, Amaral TD (2017) Low-dose radiation 3D intraoperative imaging how low can we go? An O-arm, CT scan, cadaveric study. Spine 42:E1311–E1317. https://doi.org/10.1097/Brs.0000000000002154
34. Su AW, Luo TD, McIntosh AL, Schueler BA, Winkler JA, Stans AA, Larson AN (2016) Switching to a pediatric dose O-arm protocol in spine surgery significantly reduced patient radiation exposure. J Pediatr Orthop 36:621–626. https://doi.org/10.1097/BPO.0000000000000504
35. Umebayashi D, Yamamoto Y, Nakajima Y, Fukaya N, Hara M (2018) Augmented reality visualization-guided microscopic spine surgery: transvertebral anterior cervical foraminotomy and posterior foraminotomy. J Am Acad Orthop Surg Glob Res Rev 2:e008. https://doi.org/10.5435/JAAOSGlobal-D-17-00008
36. Yoon JW, Chen RE, Han PK, Si P, Freeman WD, Pirris SM (2017) Technical feasibility and safety of an intraoperative head-up display device during spine instrumentation. Int J Med Robot 13:e1770. https://doi.org/10.1002/rcs.1770
37. Zhao J, Liu Y, Fan M, Liu B, He D, Tian W (2018) Comparison of the clinical accuracy between point-to-point registration and auto-registration using an active infrared navigation system. Spine (Phila Pa 1976) 43:E1329–E1333. https://doi.org/10.1097/BRS.0000000000002704